Dynamic deformation behavior of a face-centered cubic FeCoNiCrMn high-entropy alloy

He Junyang, Wang Qi, Zhang Husheng, Dai Lanhong, Mukai Toshiji, Wu Yuan, Liu Xiongjun, Wang Hui, Nieh Tai-Gang and Lu Zhaoping

Citation: Science Bulletin **63**, 362 (2018); doi: 10.1016/j.scib.2018.01.022

View online: http://engine.scichina.com/doi/10.1016/j.scib.2018.01.022

View Table of Contents:http://engine.scichina.com/publisher/scp/journal/SB/63/6

Published by the Science China Press

Science Bulletin 63 (2018) 362–368

Contents lists available at ScienceDirect

Science Bulletin

journal homepage: www.elsevier.com/locate/scib

Article

Dynamic deformation behavior of a face-centered cubic FeCoNiCrMn high-entropy alloy

Junyang He [a,b], Qi Wang [c,d], Husheng Zhang [c], Lanhong Dai [c], Toshiji Mukai [e], Yuan Wu [a], Xiongjun Liu [a], Hui Wang [a], Tai-Gang Nieh [f], Zhaoping Lu [a,*]

[a] State Key Laboratory for Advance Metals and Materials, University of Science and Technology Beijing, Beijing 100083, China
[b] Max-Planck-Institut für Eisenforschung, Max-Planck-Straße 1, D-40237 Düsseldorf, Germany
[c] State Key Laboratory of Nonlinear Mechanics, Institute of Mechanics, Chinese Academy of Sciences, Beijing 100190, China
[d] China Ship Development and Design Center, Wuhan 430064, China
[e] Department of Mechanical Engineering, Kobe University, 1-1, Rokkodai, Nada, Kobe 657-8501, Japan
[f] Department of Materials Science and Engineering, The University of Tennessee, Knoxville, TN 37996, USA

ARTICLE INFO

Article history:
Received 28 October 2017
Received in revised form 16 December 2017
Accepted 3 January 2018
Available online 31 January 2018

Keywords:
High-entropy alloys
Dynamic deformation
Deformation twinning
Work-hardening
Plastic stability

ABSTRACT

In this study, mechanical tests were conducted on a face-centered cubic FeCoNiCrMn high-entropy alloy, both in tension and compression, in a wide range of strain rates (10^{-4}–10^{4} s^{-1}) to systematically investigate its dynamic response and underlying deformation mechanism. Materials with different grain sizes were tested to understand the effect of grain size, thus grain boundary volume, on the mechanical properties. Microstructures of various samples both before and after deformation were examined using electron backscatter diffraction and transmission electron microscopy. The dislocation structure as well as deformation-induced twins were analyzed and correlated with the measured mechanical properties. Plastic stability during tension of the current high-entropy alloy (HEA), in particular, at dynamic strain rates, was discussed in lights of strain-rate sensitivity and work hardening rate. It was found that, under dynamic conditions, the strength and uniform ductility increased simultaneously as a result of the massive formation of deformation twins. Specifically, an ultimate tensile strength of 734 MPa and uniform elongation of ~63% are obtained at 2.3×10^{3} s^{-1}, indicating that the alloy has great potential for energy absorption upon impact loading.

1. Introduction

Recently, a new class of alloys, namely high-entropy alloys (HEAs), has attracted substantial research interests [1,2]. These alloys contain multiple metallic elements in an equiatomic or nearly equiatomic ratio and, as a result, their crystalline lattice is severely distorted and atomic diffusion is retarded [3–6]. It is noteworthy that, an equimolar quinary alloy, FeCoNiCrMn, quickly became a model HEA due to its pure simple face-centered cubic (fcc) structure and exceptional ductility [1,7–9]. Otto et al. [10] have systemically studied its tensile performance at different temperatures. While Gludovatz et al. [11] also reported its remarkable fracture toughness at the liquid nitrogen temperature, showing the presence of abundant twinning in the post-deformed samples. Later, Zhang et al. [12], by using high resolution transmission electron microscope (TEM), revealed that stacking faults nucleation and twin formation are responsible for the observed ultra-high toughness. These studies seemingly all agree that twinning is a universal mechanism when this fcc-HEA is deformed at ambient and cryogenic temperatures.

According to Zener-Hollomon parameter [13,14], $Z = \dot{\varepsilon}\exp(Q/RT)$, where $\dot{\varepsilon}$ is the strain rate, Q is activation energy, R is gas constant, and T is absolute temperature, to increase strain rate of deformation is essentially equivalent to that to lower the temperature. Therefore, high strain-rate deformation is expected to stimulate occurrence of twinning due to the suppression of dislocation activities and local stress concentration, in a manner similar to that at low temperatures. Based on the excellent properties of FeCoNiCrMn at cryogenic temperatures [10,11], we anticipate this alloy would also perform well in dynamic deformation conditions. In fact, Ma et al. [15] and Zhang et al. [16] have already made some efforts to explore the dynamic performance of HEAs. However, the particular HEAs used for their study are not single-phase but contain a mixture of fcc+bcc structures. Zhang et al. [17] have just focused on this simple fcc HEA, but only shock compression was involved, which did not provide information on plastic instability.

* Corresponding author.
E-mail address: luzp@ustb.edu.cn (Z. Lu).

https://doi.org/10.1016/j.scib.2018.01.022
2095-9273/

In the present study, we carried out a series of high strain-rate tests, not only in compression but also in tension for the first time, to systematically investigate the dynamic response of FeCoNiCrMn in order to uncover the underlying deformation mechanism. Samples with three different grain sizes were prepared to reveal roles of grain size and grain boundary-twin interaction.

2. Materials and methods

An ingot of the equiatomic FeCoNiCrMn alloy was produced via induction-melting of a mixture of pure metallic elements (purity larger than 99.8%), and re-melted four times to ensure chemical homogeneity. The final HEA ingot weighed ~3 kg with an approximately dimension of Φ 70 mm × 100 mm. The square column samples were wire-electrode cut, away from the central part to avoid as-cast macro-shrinkage and subsequently, homogenized at 1,200 °C for 12 h. For the convenience of discussion, we denote this sample as sample A. Two additional recrystallization treatments were applied to this alloy in order to obtain different grain sizes. The first one, denoted as sample B, was sample A cold rolled 50%, recrystallized at 1,100 °C for 1 h, followed by water quenching. Another one, denoted as sample C, was sample A cold rolled 50% but recrystallized at 1,000 °C for 10 min, followed by water quenching. Compressive specimens were subsequently machined from these three samples to a size of 5 mm × 5 mm × 8 mm, with their surface polished down to 2000-grid SiC paper. Tensile specimens were fine-turned to a gauge size of Φ 2.5 mm × 5 mm.

For dynamic compressive and tensile tests, standard Split-Hopkinson Pressure/Tension Bar (SHP/TB) was used [18]. For quasi-static tension tests, a CMT4105 universal electronic tensile testing machine was employed. All mechanical experiments were conducted at room temperature and for each condition at least three samples were tested to ensure reliability.

The grain size, shape, and orientation as well as twinning structure were characterized using electron back scattering diffraction (EBSD) with a ZEISS AURIGA instrument equipped with a HKL Channel 5 system operating at 20 kV. Specimens for EBSD observation were initially ground down to 5000-grit SiC paper and then, electrochemically polished using an $HClO_4$:C_2H_6O = 1:9 (in volume ratio) solution with a direct voltage of 30 V at room temperature.

For microstructural examination, a Tecnai F30 TEM operated at a 300 kV acceleration voltage was employed. TEM discs with a diameter of 3 mm were punched from the bulk sample, ground to 50 μm thickness, followed by twin-jet electro-polishing in a mixed solution of $HClO_4$:C_2H_6O = 1:9 (in volume ratio) at around −30 °C.

3. Results

Grain structures in samples A, B and C, prior to deformation are given in Fig. 1. Only few coarse grains can be observed in sample A, while the other two consist of randomly-orientated equiaxed grains, as revealed by the colors in the inverse pole figure (IPF). It is also noted that, multiple micron-scale annealing twins appear in samples B and C with a volume fraction of 6% and 15%, respectively, apparently resulted from the additional cold-rolling and aging treatment. Since it has been demonstrated before [19,20] that twin boundaries act in a similar fashion as high-angle grain boundaries during plastic deformation, we treat them equally in the grain size determination. Consequently, the average grain sizes are determined to be 450, 35 and 12 μm for samples A, B and C, respectively.

3.1. Mechanical performance

Engineering strain-stress curves of the three different samples at a dynamic strain rate of $2.1 \times 10^3\ s^{-1}$ in compression are shown in Fig. 2a. Note that even at such a high strain rate none of the three samples is fractured within the limit of the test machine (~15% strain). Despite of the minor fluctuation in the flow behavior caused by the loading shock wave, yield strengths, $\sigma_{0.2}$, were determined to be 275, 316 and 361 MPa for samples A, B and C, respectively. The yield strength appears to follow the Hall-Petch relationship, namely, a smaller grain size produces a stronger material.

To reveal the strain-rate effect, Fig. 2b shows the tensile strain-stress curves of sample B with a grain size of 35 μm tested at 4 different strain rates, i.e., 10^{-4}, 10^{-2}, 1.6×10^3 and $2.2 \times 10^3\ s^{-1}$. It is readily seen in the figure that strain rate appears to have a strong effect on strength, especially in the dynamic regime. For example, when the strain rate is raised from 10^{-4} to $10^{-2}\ s^{-1}$, the UTS increases only slightly from 577 to 610 MPa. However, once the strain rate is raised to the dynamic range of $10^3\ s^{-1}$, the UTS reaches a value of 734 MPa, with a large increment of about 124 MPa.

Also as noted in Fig. 2b, strain rate appears to have little effect on the fracture strain (ε_f) of the current HEA. All test samples exhibit outstanding ε_f over 60%, except the one tested at $1.6 \times 10^3\ s^{-1}$. However, even this sample has a respectable tensile ductility larger than 50%. Another important observation in Fig. 2b is the fact that, as the strain rate increases, both the UTS and UE increase simultaneously (as shown in Fig. 2c). It is unusual since, in most alloys, the enhancement of one of these two parameters usually leads to the expense of the other, i.e., the so-called strength-ductility tradeoff. This result suggests that the current HEA can be strengthened and toughened simultaneously as the strain rate is raised. Comparing to the cryogenic tensile performance reported in Ref. [11], strain-rate increment apparently shares similar prominent effect as reducing the temperature. In perspective, the product of strength and elongation, which is a useful material index for estimating toughness, exceeds 46,000 MPa% at a strain rate of $2.3 \times 10^3\ s^{-1}$ in tension for the current HEA. Such a high value is even comparable to that of the precipitation hardened HEA reported in

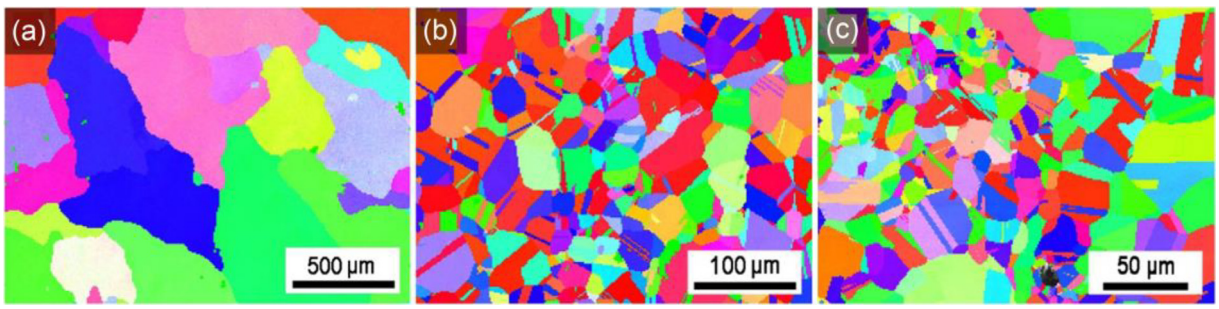

Fig. 1. EBSD IPF results exhibiting randomly-orientated grains with different grain sizes of alloys A (a), B (b) and C (c), respectively.

our previous work under quasi-static test conditions [21], suggesting its great potential for energy absorption during crush damage.

3.2. Microstructure after dynamic deformation

Microstructures of samples with different grain sizes after high strain-rate compression are presented in Fig. 3, and the images were taken on the plane parallel to the deformation direction. As shown in Fig. 3a, the grain size and morphology of sample A remain unchanged comparing to that prior to deformation. However, a majority of grains are multi-colored, indicating the formation of subgrains, probably caused by excessive dislocation motion and interaction during the dynamic loading. Fig. 3b is a higher magnification view at the grain boundary region in Fig. 3a. Substantial CSL Σ3 boundaries (denoted by the red lines in the figure), i.e., low-energy twin boundaries in fcc crystal struc-

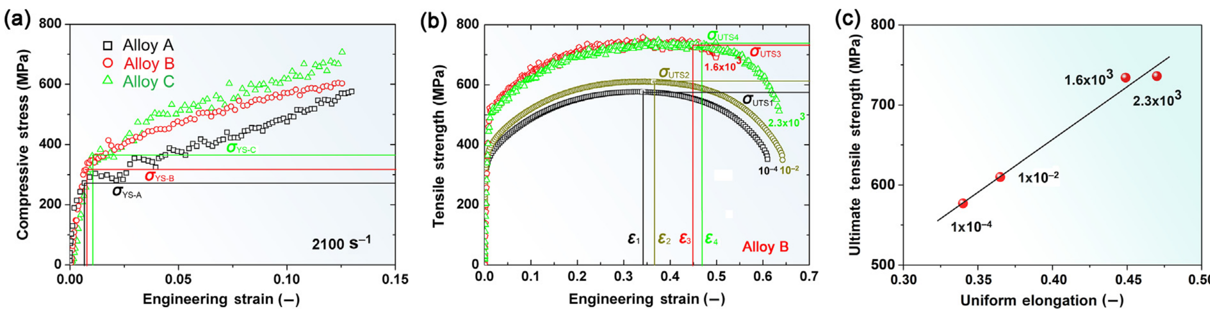

Fig. 2. Engineering strain-stress curves of alloy A, B and C in compression mode (a), alloy B in tension mode but with different strain rates (b) and ultimate tensile strength (UTS) as a function of uniform elongation (UE) in tension mode (c).

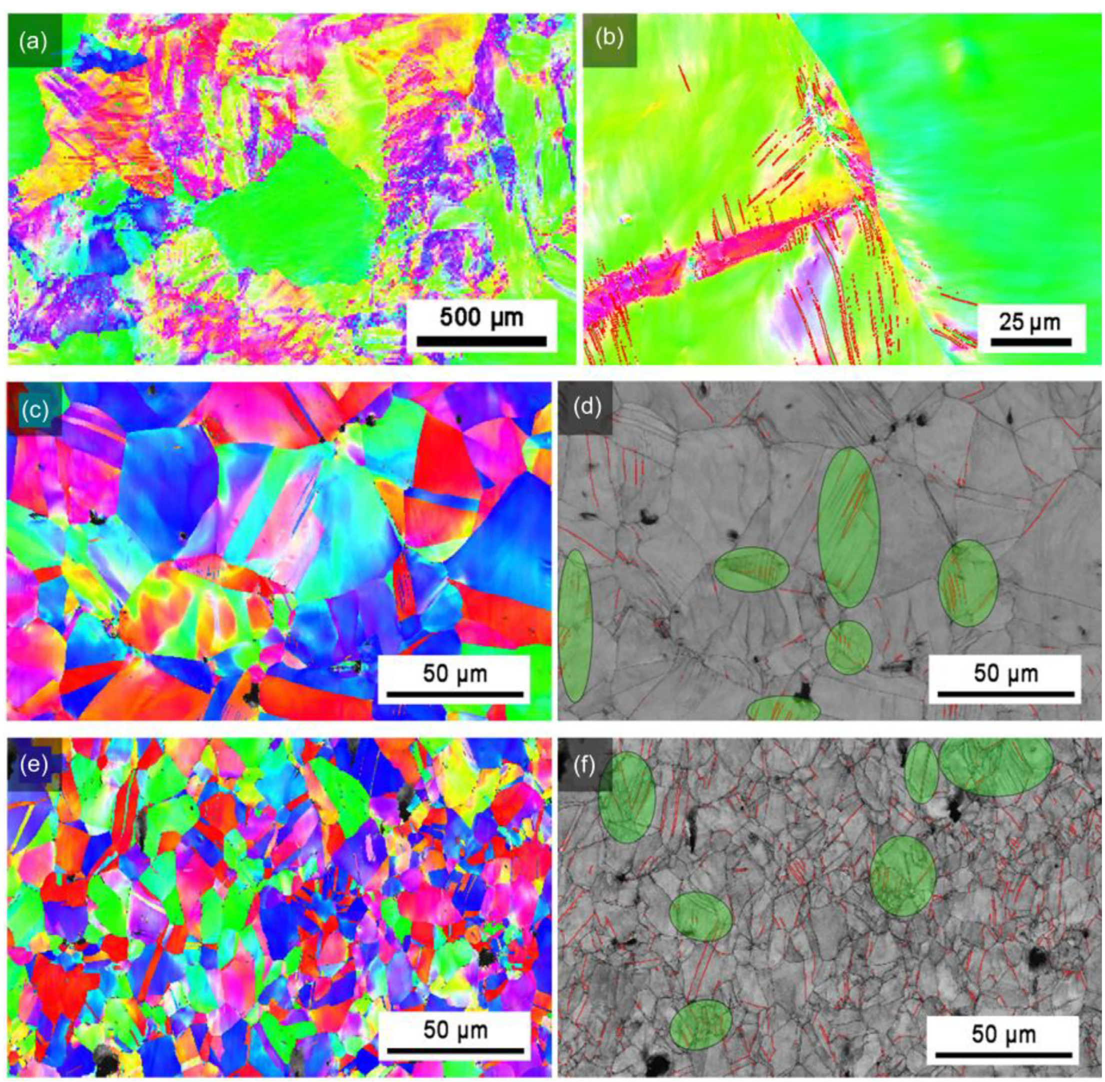

Fig. 3. EBSD results of alloys A (a, b), B (c, d) and C (e, f) after dynamic compression tests.

ture, are observed. These mechanical twins appear to form in the vicinity of grain boundaries, especially junctions where stress is easily concentrated for twinning activation. We may, therefore, conclude that dislocation slip dominantly controls the deformation process in coarse-grained sample A, but a few mechanical twins, mainly near the grain-boundary region, appear to accommodate the local strain.

In comparison with that in sample A, no complex substructure is detected in either sample B (Fig. 3c) or sample C (Fig. 3e). It may be attributed to the fact that in the two finer grained samples with larger volume fractions of grain boundary, a stronger dislocation-boundary interaction is expected, while in alloy A, grains are so large that plastic strain must be accommodated by dislocation motion within grain interior, thus results in the observed complex dislocation substructures. Σ3 twin boundaries, including those initial annealing twins, are clearly marked by red lines in the corresponding band contrast map in Fig. 3d, among which several mechanical twins are further distinguished in green circles. Apparently, most of them are developed throughout the entire grains rather than restricted within the boundary junction region, indicating that twinning plays a relatively more important role comparing to that in sample A. However, the density of deformation twins (which is difficult to quantify accurately under the resolution of EBSD) is moderate, indicating that dislocation slip still partially dominates. The microstructure of deformed sample C (Fig. 3e and f) is similar to that of deformed sample B, except with a slightly increased volume fraction of deformation twins. This result is consistent with the observation that finer grain size results in higher density of twin nucleation sites per unit grain boundary previously reported in twinning-induced plasticity (TWIP) steel [22]. To further reveal the microstructure of deformed samples, a bright field (BF) image of compressively deformed sample A is presented in Fig. 4a. Three band-like structures nearly parallel to each other are shown, and the corresponding dark field (DF) image from a zone axis of [1 1 0] is shown in Fig. 4b. It is interesting to note that each band, or bundle, actually consists of several thinner individual stacking fault layers, a precursor of mechanical twins. This observation suggests that deformation twinning is not thoroughly developed in dynamic compressed alloy A, which agrees with the EBSD result.

Microstructure of sample B deformed in tension at different strain rates was examined using EBSD IPF. It should be noted that, since the total strain is much larger (~0.5), the microstructures represent a more severe deformation. The microstructure of sample B deformed at a quasi-static strain rate of $10^{-4}\ s^{-1}$ is shown in Fig. 5a. It is obvious that all grains are elongated along the tensile loading direction. Some mechanical twins are present, but the distribution is not uniform, probably due to different grain orientations. This is not a surprise that similar phenomenon was also observed in other metallic materials, particularly in TWIP steels where twinning is readily triggered [23,24]. Nevertheless, dislocation slip still dominates tensile deformation process at low strain rates. Microstructures of sample B deformed at different dynamic strain rates in tension are shown Fig. 5b, d (i.e., 1.6×10^3 and $2.2 \times 10^3\ s^{-1}$, respectively). Grains are also stretched in the tensile direction, however, profuse mechanical twinning structures nearly fill up the majority of grains, greatly contributing to the imposed strain within grains during the severe deformation. To further view twinning structure in details, enlarged images, i.e., Fig. 5c and e, of the rectangular regions in Fig. 5b and d, respectively, were examined. It is evident that numerous twins from multi-planes are intersected, and also severely curved, indicating intensive twin interactions with each other, as well as with dislocations. Note that those dark regions along crossed bands or junctions result from highly concentrated local stresses.

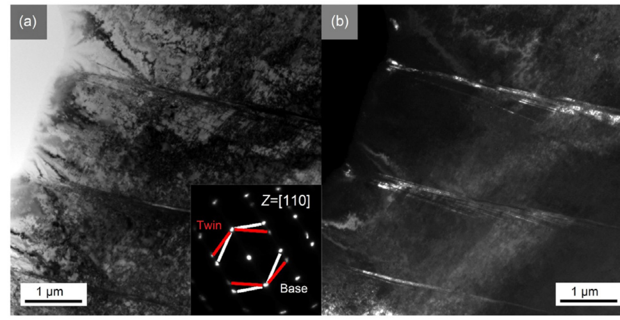

Fig. 4. TEM BF (a) and corresponding DF (b) images of sample A after dynamic compression tests showing bundle of thin twin layers.

TEM evidences of the well-developed twinning structure are presented in Fig. 6, taken the sample after being tensile-tested at $2.2 \times 10^3\ s^{-1}$ as an example. As can be seen, these stair-like bands in the corresponding BF and DF images consist of two sets of nanotwins or SFs, indicating that under the current dynamic tension condition, multiple twinning systems are activated at the same location. Accompanied with the EBSD observations, twinning is apparently a favorite deformation mode under high strain-rate tension.

4. Discussion

4.1. Grain size effect

Hall-Petch equation is usually applied to describe the strengthening caused by grain size refinement and is expressed as [25,26]:

$$\sigma_y = \sigma_0 + k_y \times d^{-1/2}, \tag{1}$$

where σ_y is the yield stress, σ_0 is the lattice friction stress, k_y is the strengthening coefficient and d is the average grain size. Based on this equation, we plot the relationship between the yield stress $\sigma_{0.2}$ and grain size d from the data in Fig. 2a, and the result is shown in Fig. 7a. The strengthening coefficient k_y is determined to be 393 MPa $\mu m^{1/2}$, lower than that measured under quasi-static test condition (~ 490 MPa $\mu m^{1/2}$) [10,27], but still fall within the general range of 300—500 MPa $\mu m^{1/2}$ for fcc alloys [28].

One of the considerations during dynamic deformation is adiabatic heating, which can effectively lower the strength, or cause softening of the test material. The temperature rising (ΔT) during adiabatic deformation can be estimated from an equation

$$\frac{\rho C_v \Delta T}{\Delta t} = \frac{\sigma \varepsilon}{\Delta t}, \tag{2}$$

where ρ is the density of the material which is around 8 g/cm^3, C_v is the specific heat capacity at constant volume and we approximately take the value from pure Ni as around 0.5 J/(g K), and Δt is the deformation duration. Therefore, ΔT at a plastic strain of ε_t can be calculated as

$$\Delta T = \frac{A}{\rho C_v} \int_0^{\varepsilon_t} \sigma \mathrm{d}\varepsilon, \tag{3}$$

where A is the fraction of energy converted into heat which is taken as ~0.9. Using Eq. (3), the maximum possible temperature rise is estimated to be 96 K when sample is tested at $2.3 \times 10^3\ s^{-1}$, which is comparable to that reported in some TWIP steels [29]. Such a temperature rise is not expected to significantly affect the yield strength of the current HEA.

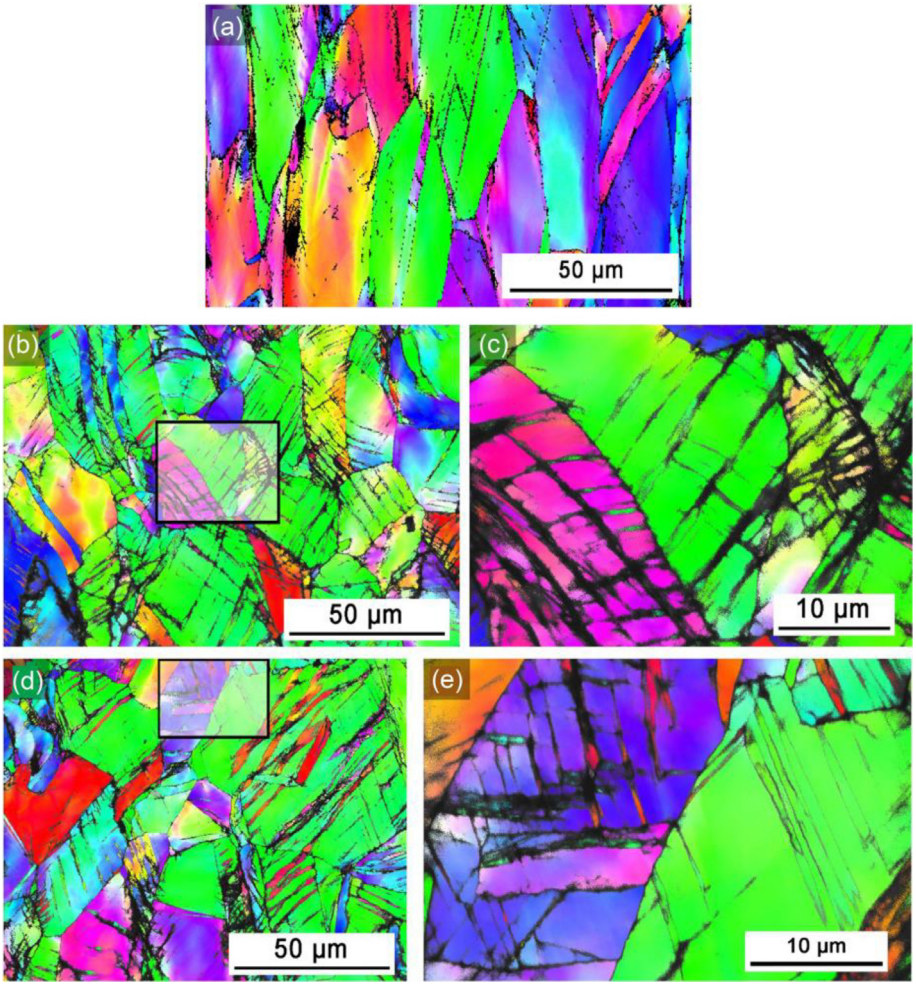

Fig. 5. EBSD results of sample B after quasi-static (a) and dynamic tension tests (b–e). (b, c)1.6 × 10^3 s^{-1}; (d, e) 2.2 × 10^3 s^{-1}.

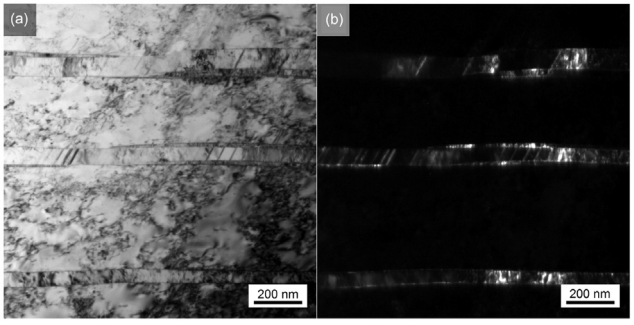

Fig. 6. TEM BF (a) and corresponding DF (b) images of sample B after dynamic tension at a strain rate of 2.2 × 10^3 s^{-1} showing multi-activated twinning system.

4.2. Strain-rate sensitivity effect

Strain-rate sensitivity (SRS) is an important parameter to describe the rate-controlling deformation of metals. In this study, the strain-rate sensitivity value of the HEA can be expressed as [30]

$$m = \left(\frac{\partial \ln \sigma_f}{\partial \ln \dot{\varepsilon}}\right)_{\varepsilon,T}, \quad (4)$$

where $\dot{\varepsilon}$ is the strain rate and σ_f is the flow stress, was evaluated and the result is plotted in Fig. 7b. It is about 0.022, which is higher than that for the traditional fcc metals and alloys in coarse-grained conditions ($m \leqslant 0.01$) [31,32]. A high m value is usually indicative of good ability to resist necking. Therefore, the current HEA is anticipated to be able to sustain a large uniform deformation during tensile deformation. In fact, it is quite consistent with the experimental results.

4.3. Work hardening behavior

The current HEA exhibits a strong work hardening capability during dynamic deformation, especially in tension as shown in Fig. 2. Here we plot the variation of work hardening rate (WHR) as a function of true plastic strain (Fig. 8a for compression and Fig. 8b for tension) and true stress (Fig. 8c only for tension). As can be seen in Fig. 8a, grain size affects little on the work hardening behavior. The work hardening rate descends rapidly in the beginning and soon saturates at a level of around (1.5 ± 1) MPa. However, it should be noted that, when strain ≤0.04, finer grains leads to larger WHR. This is because of a faster dislocation accumulation during initial stage of plastic deformation in material with more grain boundaries acting as dislocation barriers. In Fig. 8b, although the fluctuation of the two dynamic curves is larger than the quasi-static ones, it is still evident that, samples deformed at dynamic conditions have relatively larger WHR. This may be attributable to the so-called "dynamic Hall-Petch" mechanism often introduced by multiple mechanical twinning [33,34].

It was already reported that twins, especially pre-existing deformation twins, could effectively increase strength at no expense of ductility in some other fcc alloy systems [35,36].

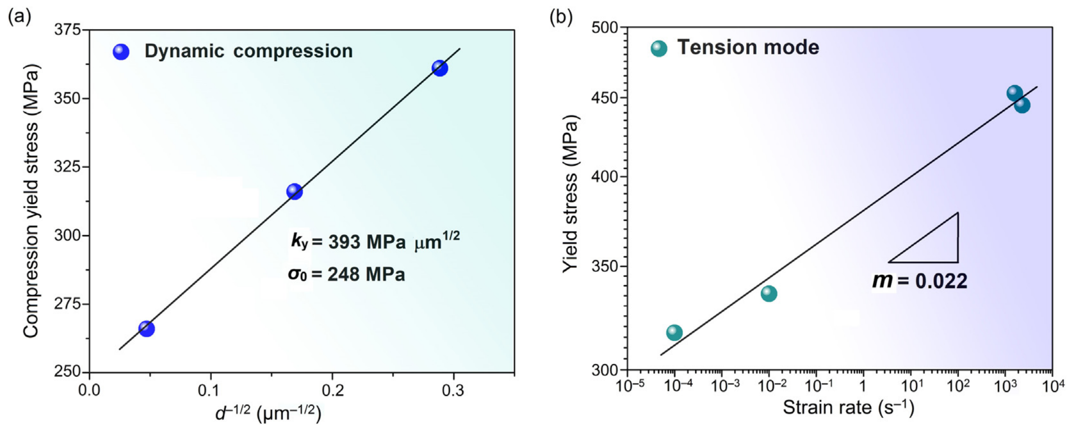

Fig. 7. Hall-Petch relationship (a) and strain-rate sensitivity (b) in the model FeCoNiCrMn HEA.

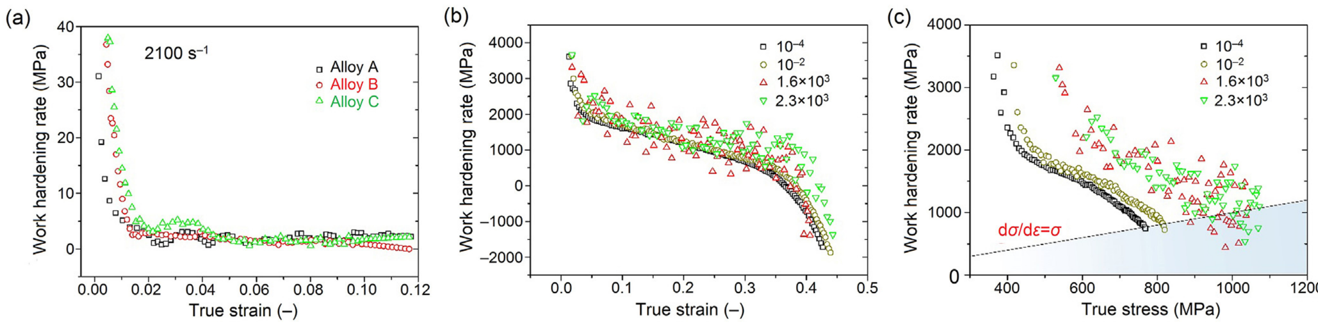

Fig. 8. Work hardening rate curve of FeCoNiCrMn HEA in compression mode (a) and tension mode (b), as well as Considere's criterion in tension mode (c).

However, twinning is difficult to activate and usually acts as an intermediate deformation mode since the stress required for twinning is much higher than that for dislocation slip. According to Narita and Takamura [37], the critical resolved shear stress required for twinning is

$$\tau_T = \gamma_{SF}/(Kb_S), \tag{5}$$

where τ_T is the critical resolved shear stress (CRSS), γ_{SF} is the stacking fault energy, K is a parameter which could be approximately determined to be 2 and b_S is the Burgers vector of the Shockley partial dislocation, for a fcc crystal it is $a[211]/6$. In the current FeCoNiCrMn alloy, $\gamma_{SF} = 30 \pm 5$ mJ/m^2 [38] and $b_S = \sqrt{6}/6a = 0.147$ nm, thus the CRSS value is estimated to be 102 MPa. If further converting the CRSS to normal stress via the Taylor factor M = 3.06, we can easily find that the value matches well with the measured uniaxial tensile yield strength of around 300 MPa in this study. This finding indicates that, due to a low stacking fault energy, twinning in the current HEA is easily activated. In fact, it occurs even at a stress near the yielding point under dynamic strain-rate conditions. The accelerated twinning deformation was clearly demonstrated in Fig. 5, especially in the two fine-grained samples.

To discuss plastic stability, in Fig. 8c, we draw a region (in blue) within which the occurrence of necking is predicted according to the Considere's criterion, i.e., when $d\sigma/d\varepsilon < \sigma$ [39]. After ignoring those post-necking data, the four experimental curves in the figure all match well with the predictions. This result also clearly indicates that deformation at dynamic strain rates effectively delays necking to a higher true (flow) stress level.

Plastic stability can also be discussed via the Hollomon equation $\sigma = K\varepsilon^N$ [40], where N is the hardening coefficient. The equation predicts that, for a work hardenable material, plastic instability occurs when $\varepsilon_{necking} \approx N$, where $\varepsilon_{necking}$ is the true necking strain [39]. From the tensile data, N values are determined to be 0.307, 0.317, 0.318 and 0.324 at strain rates of 10^{-4}, 10^{-2}, 1.6×10^3 and 2.3×10^3 s^{-1}, respectively. The corresponding necking strains are 0.295, 0.313, 0.373 and 0.387, respectively, agreeing reasonably well with equation. We may, therefore, conclude that plastic stability of the current HEA improves with increasing strain rates.

5. Conclusions

A series of high strain-rate deformation tests, both in tension and compression, were conducted on an fcc-FeCoNiCrMn HEA to systematically evaluate its dynamic response and the underlying deformation mechanism. It was found that, grain size and strain rate both played important role in the deformation process. Several key observations are described as follows.

For the grain size effect, as the average grain size reduces to ~12 μm, yield strength of the HEA increases to 361 MPa at a strain rate of 2.1×10^3 s^{-1}, almost 30% higher than that of the coarse-grained material (450 μm). The Hall-Petch relationship was obeyed even at dynamic strain rates. The hardening coefficient ($k_y = 393$ MPa μm$^{1/2}$) was found slightly lower than that in quasi-static conditions, but within the general range for fcc-metals.

For the strain-rate effect, tensile tests conducted at a wide range of strain rate show a simultaneous improvement of UTS and uniform elongation at dynamic strain rates, in a manner similar to decreasing of temperature. Specifically, a UTS of 734 MPa and

uniform deformation of ~63% are recorded at a strain rate of $2.3 \times 10^3\ s^{-1}$. In addition, a high strain-rate sensitivity value (~0.022) is obtained, indicating this HEA is resistant to local necking in tension. These results suggest that the current HEA has good potential for anti-crush and high speed shaping applications.

For the underlying deformation mechanism, at a quasi-static strain rate, dislocation slip apparently dominates, as revealed by the dislocation structure. At dynamic strain rates, on the other hand, twinning is easily triggered and overwhelmingly contributes to the total plastic strain. It is because the stress for twinning is as low as the yield strength in the current low-stacking-fault HEA. In materials with a finer grain size, the increasing grain boundary volume can further facilitate twin formation or stacking fault nucleation, as a result of enhanced local stresses in the vicinity of grain boundary.

Conflict of interest

The authors declare that they have no conflict of interest.

Acknowledgments

This work was supported by the National Natural Science Foundation of China (51671018, 51531001, 51422101, 51371003, and 51671021), 111 Project (B07003), International S&T Cooperation Program of China (2015DFG52600), Program for Changjiang Scholars and Innovative Research Team in University of China (IRT_14R05) and the Projects of SKL-AMM-USTB (2016Z-04, 2016-09, 2016Z-16). Yuan Wu acknowledges the financial support from the Top-Notch Young Talents Program and the Fundamental Research Funds for the Central Universities. Tai-Gang Nieh acknowledges the financial support by US-NSF under contract DMR-1408722.

Appendix A. Supplementary data

Supplementary data associated with this article can be found, in the online version, at https://doi.org/10.1016/j.scib.2018.01.022.

References

[1] Cantor B, Chang ITH, Knight P, et al. Microstructural development in equiatomic multicomponent alloys. Mater Sci Eng A 2004;375–377:213–8.
[2] Yeh JW, Chen SK, Lin SJ, et al. Nanostructured high-entropy alloys with multiple principal elements Novel alloy design concepts and outcomes. Adv Eng Mater 2004;6:299–303.
[3] Cantor B. Multicomponent and high entropy alloys. Entropy 2014;16:4749–68.
[4] Zhang Y, Zuo TT, Tang Z, et al. Microstructures and properties of high-entropy alloys. Prog Mater Sci 2014;61:1–93.
[5] Lu ZP, Wang H, Chen MW, et al. An assessment on the future development of high-entropy alloys: summary from a recent workshop. Intermetallics 2015;66:67–76.
[6] Miracle DB, Senkov ON. A critical review of high entropy alloys and related concepts. Acta Mater 2017;122:448–511.
[7] Wu Z, Bei H, Otto F, et al. Recovery, recrystallization, grain growth and phase stability of a family of fcc-structured multi-component equiatomic solid solution alloys. Intermetallics 2014;46:131–40.
[8] Gali A, George EP. Tensile properties of high- and medium-entropy alloys. Intermetallics 2013;39:74–8.
[9] Otto F, Yang Y, Bei H, et al. Relative effects of enthalpy and entropy on the phase stability of equiatomic high-entropy alloys. Acta Mater 2013;61:2628–38.
[10] Otto F, Dlouhý A, Somsen C, et al. The influences of temperature and microstructure on the tensile properties of a CoCrFeMnNi high-entropy alloy. Acta Mater 2013;61:5743–55.
[11] Gludovatz B, Hohenwarter A, Catoor D, et al. A fracture-resistant high-entropy alloy for cryogenic applications. Science 2014;345:1153–8.
[12] Zhang ZJ, Mao MM, Wang JW, et al. Nanoscale origins of the damage tolerance of the high-entropy alloy CrMnFeCoNi. Nat Commun 2015;10143:1–6.
[13] Zener C, Hollomon JH. Effect of strain rate upon plastic flow of steel. J Appl Phys 1944;15:22–32.
[14] Li YS, Zhang Y, Tao NR, et al. Effect of the Zener-Hollomon parameter on the microstructures and mechanical properties of Cu subjected to plastic deformation. Acta Mater 2009;57:761–72.
[15] Ma SG, Jiao ZM, Qiao JW, et al. Strain rate effects on the dynamic mechanical properties of the $AlCrCuFeNi_2$ high-entropy alloy. Mater Sci Eng A 2016;649:35–8.
[16] Zhang TW, Jiao ZM, Wang ZH, et al. Dynamic deformation behaviors and constitutive relations of an $AlCoCr_{1.5}Fe_{1.5}NiTi_{0.5}$ high-entropy alloy. Scr Mater 2017;136:15–9.
[17] Jiang ZJ, He JY, Wang HY, et al. Shock compression response of high entropy alloys. Mater Res Lett 2016;4:226–32.
[18] Chen WW, Song B. Split Hopkinson (Kolsky) bar: design, testing, and applications. Mechanical Engineering Series. New York: Springer; 2011.
[19] Bouaziz O, Allain S, Scott C. Effect of grain and twin boundaries on the hardening mechanisms of twinning-induced plasticity steels. Scr Mater 2008;58:484–7.
[20] Lee YK. Microstructural evolution during plastic deformation of twinning-induced plasticity steels. Scr Mater 2012;66:1002–6.
[21] He JY, Wang H, Huang HL, et al. A precipitation-hardened high-entropy alloy with outstanding tensile properties. Acta Mater 2016;102:187–96.
[22] Gutierrez-Urrutia I, Raabe D. Grain size effect on strain hardening in twinning-induced plasticity steels. Scr Mater 2012;66:992–6.
[23] Yang P, Xie Q, Meng L, et al. Dependence of deformation twinning on grain orientation in a high manganese steel. Scr Mater 2006;55:629–31.
[24] Meng L, Yang P, Xie Q, et al. Dependence of deformation twinning on grain orientation in compressed high manganese steels. Scr Mater 2007;56:931–4.
[25] Hansen N. Hall-Petch relation and boundary strengthening. Scr Mater 2004;51:801–6.
[26] Kato M. Hall-Petch relationship and dislocation model for deformation of ultrafine-grained and nanocrystalline metals. Mater Trans 2014;55:19–24.
[27] Sun SJ, Tian YZ, Lin HR, et al. Enhanced strength and ductility of bulk CoCrFeMnNi high entropy alloy having fully recrystallized ultrafine-grained structure. Mater Design 2017;133:122–7.
[28] Wu D, Zhang JY, Huang JC, et al. Grain-boundary strengthening in nanocrystalline chromium and the Hall-Petch coefficient of body-centered cubic metals. Scr Mater 2013;68:118–21.
[29] Curtze S, Kuokkala VT. Dependence of tensile deformation behavior of TWIP steels on stacking fault energy, temperature and strain rate. Acta Mater 2010;58:5129–41.
[30] Dieter GE. Mechanical metallurgy. New York: McGraw-Hill; 1976.
[31] Sun C, Ma J, Yang Y, et al. Temperature and grain size dependent plastic instability and strain rate sensitivity of ultrafine grained austenitic Fe-14Cr-16Ni alloy. Mater Sci Eng, A 2014;597:415–21.
[32] Wei Q, Cheng S, Ramesh KT, et al. Effect of nanocrystalline and ultrafine grain sizes on the strain rate sensitivity and activation volume: fcc versus bcc metals. Mater Sci Eng, A 2004;381:71–9.
[33] Allain S, Chateau JP, Bouaziz O, et al. Correlations between the calculated stacking fault energy and the plasticity mechanisms in Fe-Mn-C alloys. Mater Sci Eng A 2004;387–389:158–62.
[34] Allain S, Chateau JP, Bouaziz O. A physical model of the twinning-induced plasticity effect in a high manganese austenitic steel. Mater Sci Eng A 2004;387–389:143–7.
[35] Zhao YH, Bingert JF, Liao XZ, et al. Simultaneously increasing the ductility and strength of ultra-fine-grained pure copper. Adv Mater 2006;18:2949–53.
[36] Zhu YT, Liao XZ. Nanostructured metals: retaining ductility. Nat Mater 2004;3:351–2.
[37] Narita N, Takamura J. Deformation twinning in silver-and copper-alloy crystals. Philos Mag 1974;29:1001–28.
[38] Okamoto NL, Fujimoto S, Kambara Y, et al. Size effect, critical resolved shear stress, stacking fault energy, and solid solution strengthening in the CrMnFeCoNi high-entropy alloy. Sci Rep 2016;6:35863.
[39] Dieter GE. Mechanical metallurgy. 3rd ed. New York: McGraw-Hill; 1988.
[40] Hollomon JH. Tensile deformation. Trans AIME 1945;162:268–90.